Crystal structure of Rab geranylgeranyltransferase at 2.0 Å resolution

Hong Zhang[1], Miguel C Seabra[2] and Johann Deisenhofer[1]*

Background: Rab geranylgeranyltransferase (RabGGT) catalyzes the addition of two geranylgeranyl groups to the C-terminal cysteine residues of Rab proteins, which is crucial for membrane association and function of these proteins in intracellular vesicular trafficking. Unlike protein farnesyltransferase (FT) and type I geranylgeranyltransferase, which both prenylate monomeric small G proteins or short peptides, RabGGT can prenylate Rab only when Rab is in a complex with Rab escort protein (REP).

Results: The crystal structure of rat RabGGT at 2.0 Å resolution reveals an assembly of four distinct structural modules. The β subunit forms an α–α barrel that contains most of the residues in the active site. The α subunit consists of a helical domain, an immunoglobulin (Ig)-like domain, and a leucine-rich repeat (LRR) domain. The N-terminal region of the α subunit binds to the active site in the β subunit; residue His2α directly coordinates a zinc ion. The prenyl-binding pocket of RabGGT is deeper than that in FT.

Conclusions: LRR and Ig domains are often involved in protein–protein interactions; in RabGGT they might participate in the recognition and binding of REP. The binding of the N-terminal peptide of the α subunit to the active site suggests an autoinhibition mechanism that might contribute to the inability of RabGGT to recognize short peptides or Rab alone as its substrate. Replacement of residues Trp102β and Tyr154β in FT by Ser48β and Leu99β,

Addresses: [1]Howard Hughes Medical Institute and Department of Biochemistry, The University of Texas Southwestern Medical Center, Dallas, Texas 75235-9050, USA and [2]Molecular Genetics, Division of Biomedical Sciences, Imperial College School of Medicine, London SW7 2AZ, UK.

*Corresponding author.
E-mail: johann.deisenhofer@email.swmed.edu

Key words: autoinhibition, crystal structure, geranylgeranyltransferase type II, leucine-rich repeats, post-translational modification

Received: **29 October 1999**
Revisions requested: **25 November 1999**
Revisions received: **17 December 1999**
Accepted: **4 January 2000**

Published: **18 February 2000**

Structure 2000, **8**:241–251

0969-2126/00/$ – see front matter

Introduction

Many eukaryotic proteins are post-translationally modified by the attachment of lipids [1,2]. For example, isoprenoid C15 farnesyl and C20 geranylgeranyl (GG) groups are found in numerous proteins including nuclear lamins, trimeric G protein γ subunits, protein kinases, Ras, and almost all Ras-related small GTP-binding proteins. The isoprenoid groups are covalently attached via thioether linkages to cysteine residues at or near the C terminus of these proteins. Prenylation facilitates membrane association and in some cases also plays a major role in specific protein–protein interactions [3–5].

Protein prenyltransferases catalyze the transfer of the isoprenoids from either farnesyl diphosphate (FPP) or geranylgeranyl diphosphate (GGPP) to the cysteine residues of the protein substrates. The protein prenyltransferase family includes protein farnesyltransferase (FT), protein geranylgeranyltransferase type I (GGT-I) and Rab geranylgeranyltransferase (RabGGT or GGT-II) [6,7]. All protein prenyltransferases are heterodimers consisting of α and β subunits. FT and GGT-I are closely related and are often collectively called 'CaaX prenyltransferases'. Their α subunits are identical whereas their β subunits are distinct [8]. Both FT and GGT-I recognize a CaaX motif at the C terminus of their protein substrates. This motif consists of a cysteine residue that is modified in the reaction, two aliphatic residues (aa) and a C-terminal residue X (where X is any residue). In addition to the different preference for the isoprenoid substrate, FT favours methionine, serine or glutamine at the X position, whereas GGT-I prefers leucine. [5,6]. FT and GGT-I can recognize short peptides containing appropriate CaaX motifs as substrates [9–11].

Recently, the crystal structures of FT [12,13], as well as of an FT–FPP complex [14] and of a ternary complex of FT with the CaaX peptide acetyl–CVIM and the FPP analogue α-hydroxyfarnesylphosphate [15] have been determined. These structures explained the selectivity of FT for FPP and clearly showed the active site and the mode of binding of the substrates, with the cysteine sulphur of the bound peptide coordinating the active site zinc ion. The structure of the ternary complex showed that several sidechains in the active site of FT rearrange upon binding of peptide and FPP analogue [15].

RabGGT is unique in the protein prenyltransferase family. It exclusively modifies members of a single subfamily of

Ras-related small GTPases, the Rab proteins [4,16]. Rab proteins (molecular mass [M_r] ≈ 20–25 kDa) are involved in the regulation of intracellular vesicular transport in the biosynthetic secretory and exocytic/endocytic pathways [17,18]. Most Rab proteins have a flexible tail with two cysteine residues at their C termini; the cysteines are arranged in motifs such as -CC, -CXC, -CCX or -CCXX (in single-letter amino acid and where X is any amino acid). RabGGT catalyzes the transfer of two GG groups to the two cysteines at the C terminus of Rab proteins [19]. The enzyme does not recognize short peptides containing the Rab C-terminal prenylation motif, nor does it recognize the Rab protein alone [20,21]. The geranylgeranylation of Rab requires the presence of Rab escort protein (REP, M_r ≈ 72 kDa in mammals) [20,22]. The current view of the prenylation cascade is as follows: newly synthesized Rab binds REP and forms a stable Rab–REP complex with a dissociation constant of 0.15–0.4 μM [20]. RabGGT recognizes Rab–REP complexes as its protein substrate primarily through interactions with REP [20]. After prenylation, REP stays bound to the prenylated Rab and delivers Rab to its target membrane [23,24].

Here we describe the crystal structure of RabGGT at 2.0 Å resolution. The structure differs from that of FT by the addition of two discrete structural modules in the α subunit. Residue substitutions in the GGPP-binding pocket and the active site help to explain the functional differences between FT and RabGGT.

Results and discussion

Structure of RabGGT

The asymmetric unit of RabGGT crystals contains two molecules, related by local twofold symmetry; the two molecules have almost identical structures. The overall structure of RabGGT is shown in Figure 1a (see also Figure S1, Supplementary material). The α subunit of RabGGT is composed of three compact domains: a helical domain, an immunoglobulin-like (Ig-like) domain and a leucine-rich repeat (LRR) domain. The helical domain is structurally similar to the α subunit of FT with a root mean square deviation (rmsd) of 2.1 Å between 216 superimposable Cα positions in the two proteins. A structure-based alignment (Figure 2a) shows only *22%* sequence identity between FTα and RabGGTα. The 15 helices in

Figure 1

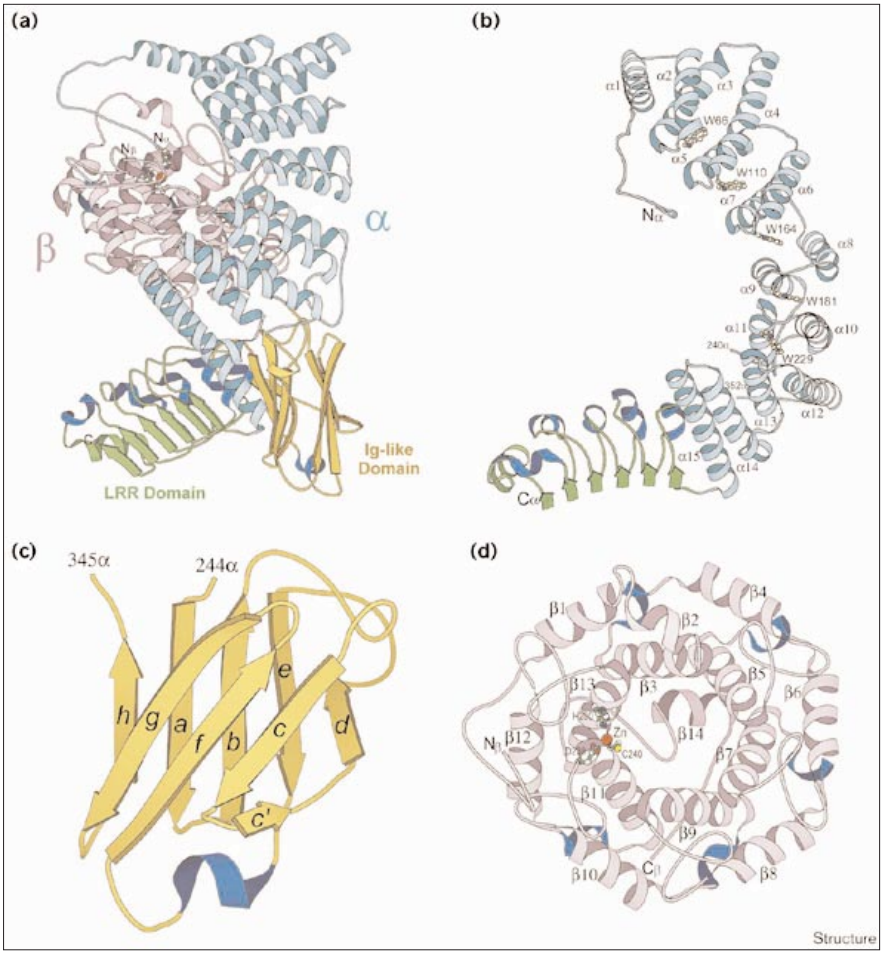

Ribbon representation of the RabGGT structure (cyan, helical domain of the α subunit; orange, Ig-like domain; green, LRR domain; purple, β subunit; blue, 3_{10} helices of all domains). **(a)** Complete structure of RabGGT. **(b)** The helical domain and LRR domain of RabGGTα in a slightly different orientation from (a). The 15 helices are numbered from α1 to α15. **(c)** The Ig-like domain of RabGGTα. The strands are labelled according to the convention in [34]. **(d)** The β subunit of RabGGT, with the zinc ion shown as a red ball and the ligands Asp238β, Cys240β and His290β in ball-and-stick representation. The helices are numbered β1–β14.

Figure 2

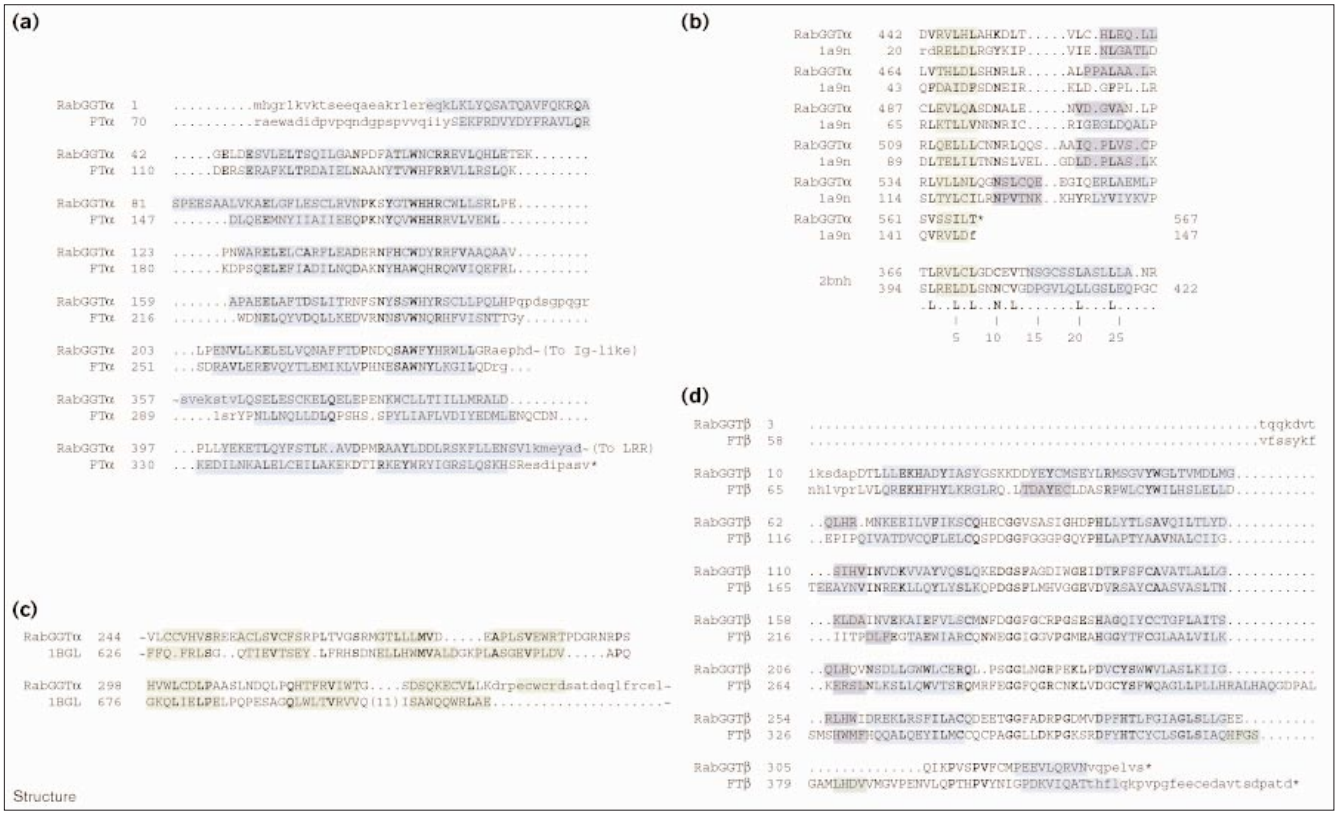

Structure-based sequence alignments. Elements of secondary structure are indicated by coloured boxes. The colour scheme used is the same as in Figure 1. **(a)** RabGGTα helical domain against FTα. **(b)** RabGGTα Ig-like domain against domain 4 in β-galactosidase (1BGL). **(c)** RabGGTα LRR domain against U2A′LRR (1a9n). Two LRRs with lengths of 28 and 29 residues each from porcine ribonuclease inhibitor (2bnh) are also aligned. The LRR consensus sequence motif is show at the bottom. **(d)** RabGGTβ against FTβ.

the helical domain (α1 to α15; Figure 1b) form a crescent-shaped right-handed superhelix. A similar fold has been found in several other proteins including lipovitellin [25,26], bacterial muramidase [27], and more recently in the tetratricopeptide repeat (TPR) region of protein phosphatase 5 [28]. Most likely, an evolutionary relationship exists between the repeat sequences in prenyltransferase α subunits and those in TPRs [29].

The presence of an Ig-like domain and an LRR domain in the α subunit distinguish RabGGT from FT and GGT-I. The Ig-like domain comprises residues 244α to 345α and is folded into an eight-stranded β sandwich (Figure 1c). All eight cysteine residues of the domain are in the reduced state. The domain is inserted between helices α11 and α12, and connected to the helical domain by two loops the high B factors of which indicate flexibility. One face of the domain (strands *h*, *a*, *b*, *e*) is packed against the LRR domain. The Ig-like domain has few other intramolecular contacts but interacts with three neighbouring molecules in the crystal; this suggests that the observed orientation is, at least in part, determined by crystal contacts. A DALI search [30] for structures similar to the Ig-like domain gives Z-scores of 6.4 for β-galactosidase domain 4 [31], 6.2 for the CH2 domain (residues 238–338) of an IgG crystallizable fragment (Fc) [32], and 3.4 for the C2 domain of synaptotagmin [33]. The sequence identity between 86 aligned residues in the RabGGT Ig-like domain and domain 4 of β-galactosidase is 19% (Figure 2b), indicating that these two domains might be evolutionarily related. Without the eighth strand, the Ig-like domain in RabGGTα would belong to the *h*-type immunoglobulin fold [34].

The second additional domain, the LRR domain, comprises residues 443α to 567α, including the C terminus of the α subunit (Figure 1b). The sequence of this domain contains five LRRs with lengths varying from 22–27 residues (Figure 2c). The LRR domain folds into a right-handed superhelix of alternating β strands and 3_{10} helices (α helix in the last repeat); the axis of the superhelix is slightly curved towards the β-sheet side. The conformation of each individual LRR unit is similar to that observed in porcine ribonuclease inhibitor (PRI) [35].

Figure 3

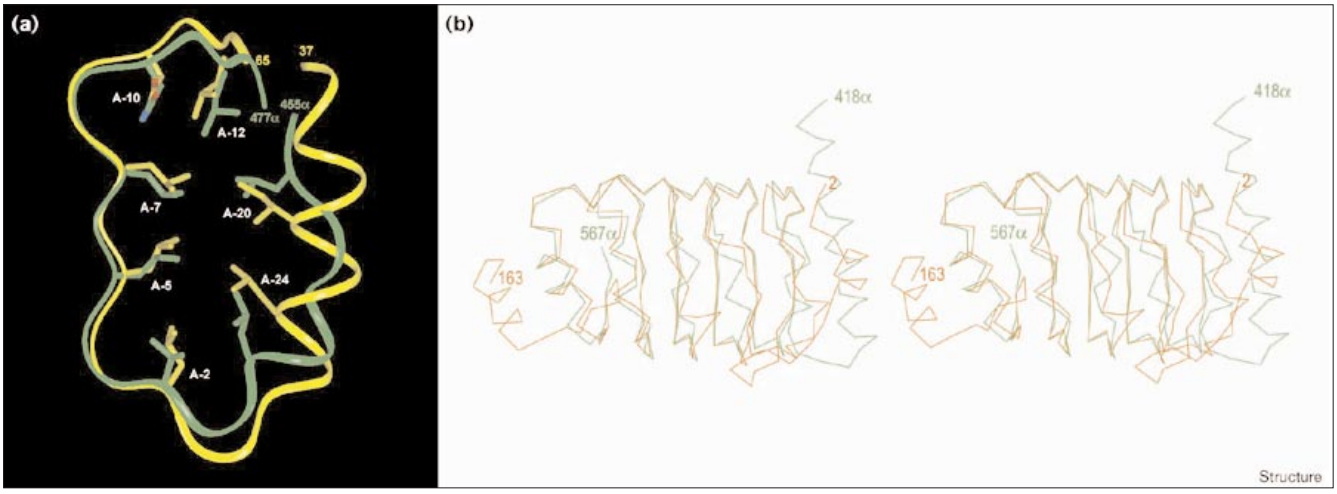

Comparison of RabGGT LRR domain with other LRR structures. **(a)** Superposition of one LRR unit from RabGGT (shown in green) with one from PRI (shown in yellow). The positions are marked as in the consensus sequence described in [35]. **(b)** Stereoview Cα trace of the RabGGT LRR domain superimposed with U2A′LRR [38]. RabGGT is coloured green and U2A′LRR is coloured orange. The first and last residues of each domain are labelled.

Especially the β-strand regions and the αα, $\alpha\beta_E$, and $\beta_P\gamma$ turns (nomenclature as in [35]) of the two structures superimpose well, except for the last repeat (Figure 3a). With an average length of 24 residues the LRR units in the RabGGT LRR domain are shorter than those in PRI (28–29 residues per repeat), and represent the most populated subfamily of LRRs [36,37]. Extended loops, followed by short 3_{10} helices, substitute for the longer helical regions found in PRI; this causes the superhelix of the RabGGT LRR domain to be less curved than in PRI. Recently, the three-dimensional structure of another LRR-containing protein, the spliceosomal U2A′LRR in complex with U2B″ and a fragment of U2 RNA [38], was determined. Like the RabGGT LRR domain, U2A′LRR contains five typical LRRs, and their overall structures are very similar as indicated by an rmsd of 1.2 Å over 116 superimposable Cα positions (Figure 3b). Remarkably, the last repeat, which has a conformation rather different from the rest of the repeats, adopts very similar conformations in the two structures. The N-terminal helix flanking the first LRR in U2A′LRR is also in approximately the same place as helix α15 in RabGGT (Figure 3b). The hydrophobic face of helix α15 of RabGGT is packed tightly against the hydrophobic interior of the LRR domain at the N-terminal end (Figure 1b). This suggests that the position of the LRR domain is fixed relative to the helical domain of RabGGTα.

The β subunit of RabGGT contains an α–α barrel made up of 12 α helices (Figure 1d); it is very similar to the α–α barrel in the β subunit of FT [12] with an rmsd of 1.4 Å between 280 superimposable Cα positions. With 30% identity (Figure 2d), the sequences of the β subunits of FT and RabGGT are more conserved than those of their α subunits. The α–α barrel fold has also been observed in other protein structures, including squalene–hopene cyclase [39], complement component C3d [40] and endoglucanase [41]. The β subunit in RabGGT is smaller than the β subunit in FT (331 residues in RabGGTβ versus 437 residues in FTβ). It lacks the first α helix and the C-terminal long loop compared with FTβ. The centre of the α–α barrel forms a funnel-shaped pocket lined with mostly aromatic residues. The bottom of this barrel is blocked by a turn, followed by a short α helix near the C terminus of the β subunit, whereas the top of the barrel is open. The crescent-shaped helical domain in RabGGTα embraces the β subunit around half its circumference close to the open end of the barrel (Figure 1a), whereas the Ig-like and LRR domains do not make contacts with the β subunit. The 3_{10} helix side of the LRR domain and the bottom of the α–α barrel of the β subunit form a pronounced groove (Figure 1a; see also Figure S2, Supplementary material).

Zinc-binding site

The first direct evidence for the presence of an intrinsic zinc ion in RabGGT was the observation of the zinc edge in the X-ray absorption spectrum of a RabGGT crystal (data not shown). Anomalous difference Fourier maps showed the location of the zinc ion in the β subunit, where it is coordinated by Asp238β, Cys240β and His290β (Figure 4) in a fashion similar to that observed in FT. The fourth ligand of the zinc ion is residue His2α of the same RabGGT molecule (Figure 4). The N-terminal region of

the α subunit binds to the β subunit in an extended conformation with His2α coordinating the zinc ion, and Lys6α forming an ionic interaction with Asp272β. It also contacts residues 283β–285β, which are part of the long loop connecting helices β12 and β13. The N termini of both α and β subunits in RabGGT are modified (M Seabra, unpublished observations), and the density at the N terminus of the α subunit can be modelled as a formylated methionine (Figure 4).

In the crystals of unliganded FT the C-terminal region of a neighbouring β subunit binds to the active site [12]. This intermolecular interaction is most probably because of crystal packing because it does not involve the catalytic zinc ion and is absent in the isomorphous crystals of an FT–FPP complex [14]. In contrast, the interaction between the N-terminal region and the active site in RabGGT includes direct binding of His2α to the zinc ion, and is intramolecular. The high B factors and poorly defined density of residues 8–26α indicate that the connection between the N-terminal region of RabGGTα and the main body of the α subunit is mobile, so that it can move out of the way upon binding of substrate peptide. The binding of the N-terminal region to the active site might be autoinhibitory and prevent binding of short substrate peptides to RabGGTα.

Figure 4

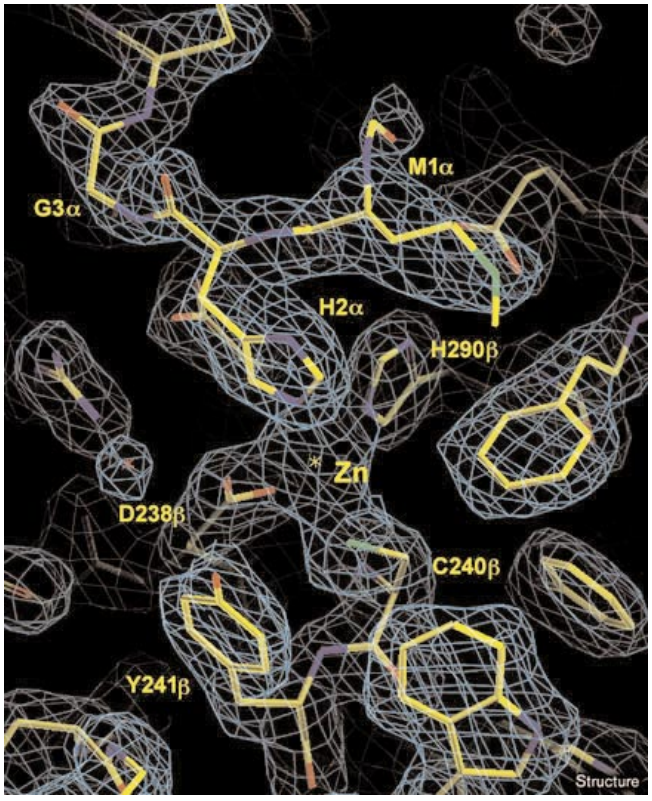

Electron density and atomic model in around the active site with the zinc ion and its protein ligands. The map was calculated with SIGMAA-weighted $2F_o–F_c$ coefficients and final model phases; the contour level is at 1σ.

Comparison of the peptide-binding sites of FT and RabGGT

A superposition of the RabGGT active site with both unliganded and liganded FT is shown in Figure 5. In the crystal structure of the complex of FT with substrates [15] the cysteine sulphur of the bound CVIM peptide coordinates the active site zinc ion. The hydrophobic sidechains of isoleucine and methionine are in the pocket lined with the FT sidechains of Trp102β, Trp106β, Tyr361β, His149β, Ala151β and Pro152β; the isoleucine sidechain is also in van der Waals contacts with the FPP isoprenoid. The mainchain of the bound peptide interacts with FT as well: the isoleucine carbonyl oxygen forms a hydrogen bond with the guanidinium group of Arg202β, and the terminal carboxylate interacts with Gln167α. The sidechains of some active-site residues, including Tyr166α, Arg202β and Glu198β, adopt different conformations in unliganded FT [12] and in FT with bound peptide and lipid substrates [15].

Several residues in the peptide substrate binding pockets of FT and RabGGT are different (Figure 5); these residues are highly conserved within members of the FT and RabGGT families. Ala151β and Pro152β in FT form part of the pocket that accommodates the methionine sidechain of the bound CVIM peptide; they are changed to leucine 96β and Tyr97β in RabGGT, respectively, which would clash with the methionine sidechain (Figure 5). Gln167α in FT, which forms a hydrogen bond with the carboxylate of the bound CVIM peptide, is replaced with Gly108α in RabGGT. In addition, sidechains of Tyr107α and Glu140β in RabGGT adopt conformations drastically different from those of the corresponding residues Tyr166α and Glu198β in the unliganded FT; their conformations are more similar to those in the FT–substrate complex (Figure 5).

These structural differences between the active sites of FT and RabGGT weaken the interactions between the tetrapeptide and RabGGT. Further reasons for the inability of RabGGT to bind and prenylate cysteine-containing tetrapeptides or monomeric Rab proteins might be the positions of cysteines at, or 1–2 residues away from, the C terminus of most Rab proteins. As the cysteine must bind to the zinc ion, only 0–2 additional residues are interacting with the enzyme. For the intramolecular interaction of the N-terminal region of the α subunit with the active site to be disrupted and replaced, substrate in high local concentration is needed. Such a high local substrate concentration is likely to exist in the complex of Rab–REP with RabGGT.

Prenyl-binding site

The α–α barrel of the RabGGT β subunit contains a central cavity that is lined with several hydrophobic

Figure 5

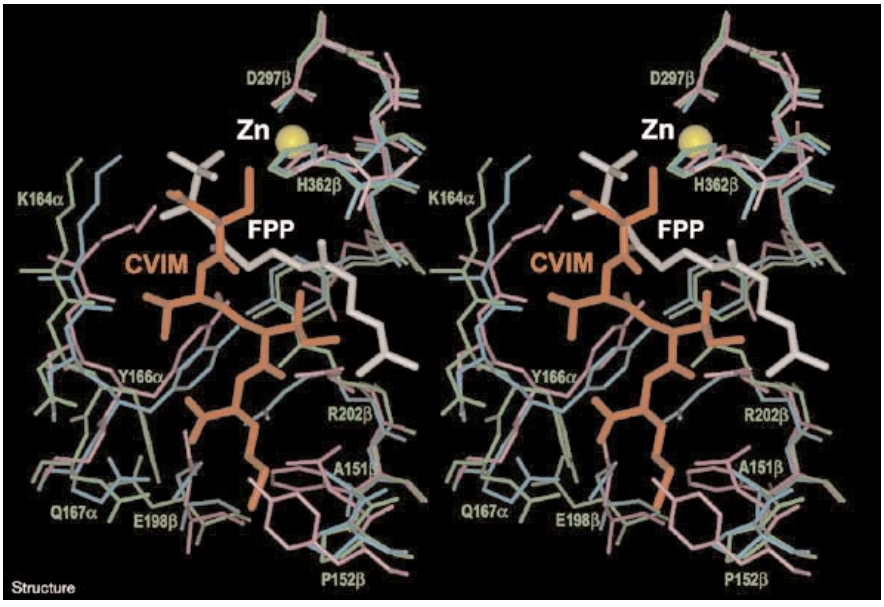

Stereo diagram of RabGGT active site, superimposed with substrate-free FT ([12], PDB code 1FT1), and FT–substrate ternary complex ([15], PDB code 1QBQ). RabGGT is coloured magenta; substrate-free FT, green; liganded FT, blue; FPP, gray; and the peptide substrate, red. Selected residues of unliganded FT are labelled.

residues including Trp52β, Phe147β, Tyr195β, Trp243β, Trp244β, Phe289β and Phe293β. A positively charged cluster formed by Arg232β, Lys235β and Lys105α is located near the opening of the cavity, close to the interface with the α subunit, and about 9 Å from the active site zinc ion. Both the hydrophobic cavity and the positively charged cluster are also present in FT. In the structure of the FT–FPP complex [13,14], the FPP binds with its hydrophobic tail to the interior of the cavity and with the diphosphate head group to the positively charged cluster. Residues from the α subunit also contribute to the diphosphate-binding site.

The most noticeable difference between the prenyl-binding cavities of FT and RabGGT is the substitution of residues Trp102β and Tyr154β of FT by residues Ser48β and Leu99β in RabGGTβ. This leads to a significantly wider and deeper cavity in RabGGT (Figure 6a). We have modelled a GGPP molecule in the pocket at a position similar to that observed in the structure of the FT–FPP complex [13,14], with the diphosphate moiety near the positively charged cluster and the tail of the GG group near Leu99β (Figure 6b). A tyrosine residue at position 99β would clash with the modelled GGPP tail, whereas a tryptophan at position 48β does not seem to interfere. It is possible, therefore, to model GGPP with two slightly different conformations: one conformation would have the GG tail near Ser48β, and the other would have the tail near Leu99β. A multiple alignment shows that in the GGT-Iβ sequence family, the tyrosine at the position corresponding

Figure 6

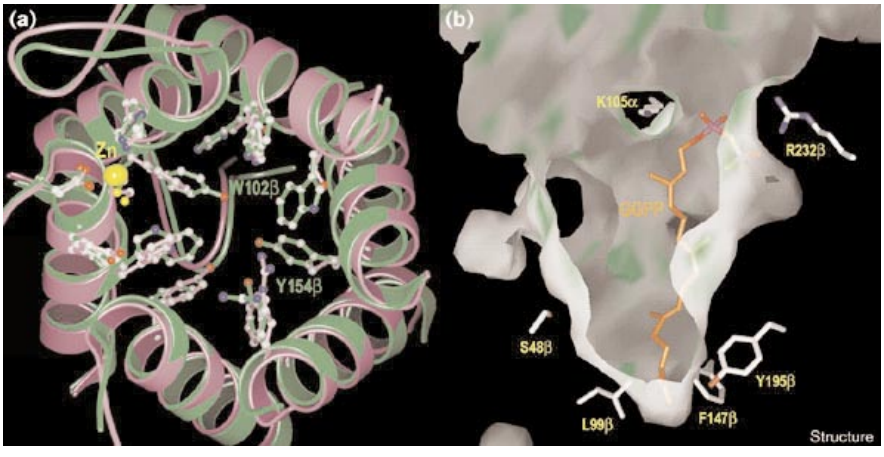

Prenyl-binding pocket. **(a)** Comparison of the prenyl binding pockets of RabGGT (magenta) and FT (green). The sidechains of several relevant residues are shown in ball-and-stick representation. Residues W102β and Y154β of FT are labelled; these residues correspond to S48β and L99β of RabGGT, respectively. **(b)** Surface representation of the GGPP-binding pocket of RabGGT with a hypothetical GGPP model. Key residues determining the size of the pocket and the phosphate-binding site are labelled. The peptide-binding site, including the zinc ion, is cut away for clarity.

to Tyr154β in FT is conserved, whereas the residue corresponding to Trp102β in FT is replaced by smaller residues such as aspartic acid or serine (data not shown). In the RabGGT family, both positions are occupied by smaller residues. The distinct conservation pattern at these two positions might serve as a signature for the three protein prenyltransferase subfamilies.

Two other highly conserved residues in FT or GGT-I α subunits, Tyr131α and Gln167α, are Ala63α and Gly108α, respectively, in RabGGTα. These two residues are located at the interface of the α and β subunit near the lipid-binding site. The role of these two residues remains to be examined.

The double prenylation mechanism

Previous studies on mammalian FT indicate that farnesylation proceeds via an ordered sequential mechanism [42,43]. FT first binds FPP, which then reacts with the peptide substrate to form the product. The product release is the rate-limiting step in this sequence [44]. After prenylation, the sulphur atom of the produced thioether remains coordinated to the metal ion in the FT enzyme–product complex [45], and the prenylated peptide product does not dissociate from the enzyme unless additional substrate is provided [46].

A recent study showed that RabGGT, like GGT-I, possesses a single GGPP-binding site, despite the fact that the enzyme catalyzes double GG transfer [47]. Consistent with this result, there is only one positively charged cluster that could bind a diphosphate moiety in the RabGGT crystal structure, although the lipid-binding pocket could accommodate GG groups in alternative conformations. Residues Tyr241β and Lys105α are likely to play a crucial role in the correct positioning of the first and the second phosphate and thus of the GGPP C1 atom near the protein substrate thiol for the subsequent nucleophilic attack. Mutations of the two corresponding residues, Tyr310β of yeast FT and Lys164α of rat FT, completely abolished enzyme activity [48,49].

Two possible scenarios could occur after the first GG transfer is accomplished. First, the monoprenylated product could remain bound to the enzyme, and the diphosphate head group dissociates from the active site. As soon as the diphosphate-binding site becomes vacant, a second GGPP might be able to bind to the enzyme. The conversion of a thiolate-S ligand to a more weakly bound thioether-S ligand might drive ligand reorganization at the metal centre, in which the other free cysteine at the Rab C terminus might become liganded to the zinc and ready for the second prenylation reaction. Another scenario is that after the first prenylation, the monoprenylated peptide dissociates from the active centre temporarily, but because the catalytic ternary complex is still intact through interactions between RabGGT and the Rab–REP complex, the dissociated peptide could bind to the active site again for the second prenylation. In both scenarios, rearrangement of the C-terminal peptide of Rab after the first prenylation has to take place for prenylation of the second cysteine. This requires less specific and more flexible binding of the peptide in RabGGT than in FT and explains the necessity for recognition and binding between Rab and RabGGT at other sites.

The most striking difference between RabGGT and FT or GGT-I is the presence of two additional domains in the α subunit, the Ig-like domain and the LRR domain. Both domains appear in many proteins and mostly participate in protein–protein interactions [34,50]. In RabGGTα the two domains could provide part of the necessary interactions with Rab proteins for the double prenylation to proceed. Both the Ig-like domain and the LRR domain are located opposite from the active site, however, so that Rab with its C terminus bound to the active site of RabGGT could not make contact with either domain. The observation that Rab has to form a complex with REP before binding to RabGGT [20] suggests that REP is likely to make this contact.

In addition, a different kind of steric restraint might prevent Rab from interacting with RabGGT directly: the source of cellular GGPP is probably either a membrane pool or GGPP synthetase. In order to be able to take up lipid before and during double prenylation, RabGGT needs to keep its active site accessible for contacts with either the membrane or GGPP synthetase. This might be another reason why Rab itself does not form contacts with RabGGT near the active site, and requires to form the Rab–REP complex in order to interact with RabGGT at sites remote from the active site.

REP is structurally and functionally related to another Rab-binding protein, Rab GDP dissociation inhibitor (RabGDI) [4,51]. RabGDI is postulated to extract Rab proteins from acceptor membranes, and to recycle them through the cytosol back to donor membranes [17,18]. The three-dimensional structure of RabGDI is similar to that of FAD-dependent flavoproteins [51]. There is no indication that RabGDI binds FAD, however, and the region equivalent to the FAD-binding pocket is a shallow groove. It is possible that the digeranygeranyl groups bind to this groove. Given the high similarity between RabGDI and REP, we assume that they interact similarly with Rab proteins. Compared with RabGDI, REP has an insertion of ~140 amino acids in the middle of the protein and about 70 more residues at the C terminus. These additional regions might mediate the interaction of REP with RabGGT; they might also contribute to the binding of both prenylated and unprenylated forms of Rab proteins by REP.

From the protein sequences available so far, it can be seen that the Ig-like and LRR domains are present only in the α subunits of RabGGTs from mammals, *Arabidopsis thaliana* and *Caenorrhabitis elegans*, but not in those of yeast. Also, the yeast counterpart of REP does not contain the unique 140 amino acid insert [52]. This suggests that the interaction between REP or the REP–Rab complex with the enzyme in yeast might be distinct from that in the higher eukaryotes.

Identification of the potential binding regions in the enzyme and protein substrate might have implications beyond mechanistic insights into the prenylation reaction. Defects in Rab prenylation are the cause of the retinal degenerative disease choroideremia [22,53]. The disease is caused by loss-of-function mutations in REP1, which is one of the two known human REP genes, REP1 and REP2. The phenotype is restricted to the retina because REP1 function is compensated in most cell types by the closely related REP2 [54]. In choroideremia cells, in which only REP2 is active, one Rab (Rab27) remains selectively unprenylated. It appears, therefore, that the molecular defect is an inability to prenylate efficiently a specific substrate of RabGGT, namely the REP2–Rab27 complex [55,56]. This could be because of a low affinity REP2–Rab27 interaction or a low affinity of the complex for the enzyme. The crystal structure of RabGGT represents the first step towards understanding the recognition of REP–Rab and the complex mechanism of double prenylation catalyzed by RabGGT. This will lead to understanding of the molecular defect in choroideremia.

Biological implications

Rab geranylgeranyl transferase (RabGGT) is unique in the protein prenyltransferase family because it recognizes only a Rab–Rab escort protein (REP) complex as its protein substrate, and because it catalyzes double prenylation of Rab. The structure of RabGGT reveals an unusual architecture of four distinct domains, each with a different fold. The β subunit is the major catalytic component; it is composed of an α–α barrel fold, which has been found in several other enzymes, among them protein farnesyltransferase (FT). The α subunit consists of three domains: an α-helical domain structurally similar to the α subunit of FT; an immunoglobulin-like domain; and a leucine-rich repeat domain. Most likely, these additional domains are involved in the recognition of the REP–Rab complex, especially in the interaction with REP, and perhaps with other proteins as well.

The high-resolution structure of RabGGT provides details of the active site and the substrate-binding pockets that enable us to gain new insights into the substrate-binding specificity and, in particular, the double prenylation mechanism. The substitution of residues Trp102β and Tyr154β of FT by residues Ser48β and Leu99β in RabGGT is probably the main determinant of the different prenyl binding specificity of the two enzymes. The presence of only one possible diphosphate-binding site suggests that the binding and the correct positioning of the second geranylgeranyl diphosphate can only occur after the dissociation of the first diphosphate group. The N-terminal region of the α subunit binds to the active site in the β subunit in an autoinhibitory fashion. The RabGGT structure reported here suggests further biochemical and mutagenesis studies of the interaction of RabGGT with the REP–Rab complex, of the double prenylation mechanism and of the functional role of autoinhibition.

Materials and methods

Protein expression and purification

RabGGT was expressed in Sf9 cells co-infected with baculovirus encoding the α and the β subunit, and partially purified using ion exchange chromatography (Q-Sepharose, Pharmacia) and gel filtration (Superdex 200, Pharmacia), as described previously [54,57]. To obtain highly purified and homogeneous protein suitable for crystallization experiments, RabGGT was further subjected to ion exchange and hydrophobic interaction chromatography. The pooled RabGGT fractions from the Superdex 200 column were loaded on a Mono Q HR10/10 column (Pharmacia) equilibrated with 50 mM Bis-Tris (pH 6.5), 150 mM NaCl and 1 mM DTT. The protein was eluted using a 160 ml linear gradient of 150–350 mM NaCl. Next 4 M $(NH_4)_2SO_4$ was added to the pooled RabGGT fractions until the final concentration of $(NH_4)_2SO_4$ was 0.6 M. This material was loaded on a Phenyl Superose HR10/10 column (Pharmacia) that had been equilibrated in buffer containing 50 mM Hepes (pH 7.2), 0.6 M $(NH_4)_2SO_4$ and 1 mM DTT. The column was then washed with a 80 ml gradient of 0.6–0.24 M $(NH_4)_2SO_4$. The protein was concentrated to 15 mg/ml, frozen in liquid nitrogen and stored at −80°C in a buffer containing 20 mM Hepes (pH 7.2), 20 mM NaCl, 10 mM $MgCl_2$, 10 mM NaH_2PO_4 and 5 mM DTT. Usually 5–10 mg pure RabGGT were obtained from 1 l of Sf9 cell culture.

Protein crystallization

RabGGT crystals were grown by the hanging drop vapor diffusion method at 21°C. A 2 μl aliquot of 5–10 mg/ml of RabGGT in storage buffer was mixed with 2 μl precipitant solution (0.1 M Na-acetate, 0.25 M Mg-acetate, 10 mM NaH_2PO_4, 6% ethylene glycol and 17–21% PEG8000, pH 5.5) and equilibrated against a reservoir containing 0.7 ml precipitant solution. Crystals usually appeared overnight and reached a maximum size of 0.7 mm × 0.3 mm × 0.1 mm in one week. The crystals have the symmetry of space group P1 with two molecules in the asymmetric unit. Unit-cell dimensions are a = 57.86 Å, b = 77.44 Å, c = 121.78 Å, α = 74.60°, β = 79.91° and γ = 67.89°. The solvent content of the crystals is 42%. After having grown for 8–10 days, the crystals were harvested in a stabilization solution (0.1 M BES, 0.25 M Mg-acetate, 15% PEG8000, 3% ethylene glycol, pH 7.2) for heavy-atom derivatization. Before collecting X-ray diffraction data, crystals were cryoprotected in stabilization solution supplemented with 5–30% PEG400, mounted on cryoloops (Hampton, Riverside, CA) and frozen in liquid propane.

X-ray data collection and structure determination

X-ray diffraction data were collected on an Raxis IIC image plate system with graphite-monochromatized CuKα X-rays produced by a Rigaku RU-300 generator, and on a nine-element CCD detector at beamline 19ID at the Advanced Photon Source (APS), Argonne National Laboratory. The synchrotron data were collected at a wavelength of 1.0084 Å. All X-ray diffraction data were measured at −180°C. Raw images were processed using the HKL package [58]. The conventional heavy-atom derivatized crystals were prepared by soaking the crystals in the stabi-

Table 1

Crystal data and phasing statistics.

	Native I*	Native II†	Xe derivative†	Ir derivative*	Pt derivative*	Hg derivative*
Resolution limits (Å)	2.0	2.25	2.6	2.5	2.5	2.5
R_{sym}‡	0.063 (0.58)	0.062 (0.50)	0.098 (0.34)	0.051 (0.19)	0.071 (0.69)	0.072 (0.28)
Observations	446,152	144,448	187,269	268,007	218,699	244,124
Unique reflections	118,808	78,800	54,221	63,630	61,166	64,091
Completeness (last shell)	93.4 (86.1)	86.5 (55.1)	93.2 (63.9)	97.9 (92.3)	92.9 (80.8)	98.1 (94.0)
$\langle I \rangle / \sigma(I)$ (last shell)	23.2 (2.33)	10.9 (2.01)	17.7 (4.12)	30.6 (7.61)	17.9 (1.44)	22.4 (4.15)
Heavy-atom concentration	–	–	300 psi	10 mM	sat.	5 mM
Soak time (h)	–	–	0.2	2.5	3	0.5
Number of sites	–	–	5	9	6	8
$\Delta F/F$§	–	–	0.20	0.24	0.20	0.24
F_H/E#	–	–	0.75	0.64	0.61	0.60
R_{cullis}¶	–	–	0.90	0.92	0.92	0.93
<FOM>¥	0.389					

*Data were collected at APS, Argonne National Laboratories, Beamline 19ID. †Data were collected on RAXIS-II image plate with Rigaku RU300 rotating-anode generator. ‡$R_{sym} = \Sigma_j | I_j - \langle I_j \rangle | / \Sigma_j I_j$, where $\langle I_j \rangle$ is the average intensity of reflection j for its symmetry equivalents; values in parentheses are for the highest resolution shell. §$\Delta F/F = \Sigma_j | F_{PH} - F_P | / \Sigma_j F_P$, where F_{PH} and F_P are the derivative and native structure-factor amplitudes, respectively. #$F_H/E = \Sigma_j | F_H |^2 / \Sigma_j | E |^2$ in the phasing power of the derivative; F_H is the calculated heavy-atom structure-factor amplitude and E is the lack of closure error. Phases were calculated to 2.5 Å resolution. ¶$R_{cullis} = \Sigma j | F_{PH} \pm | F_P = F_H | | / \Sigma_j | F_P \pm F_H |$. ¥<FOM> is the mean figure of merit.

lization solution containing heavy atom compounds for various periods of time. Xenon-derivatized crystals were prepared in a specially designed xenon chamber (courtesy of Z Wang) following a procedure similar to that described by [59]: a RabGGT crystal was mounted on the cryoloop after cryoprotection, and was inserted into the xenon pressure cell containing a drop of the cryoprotectant solution to maintain humidity. The cell was then pressurized with 300 psi xenon gas for 10–20 min after which the crystal was quickly frozen in liquid propane within a few seconds of complete depressurization.

The RabGGT structure was determined by a combination of multiple isomorphous replacement (MIR) and molecular replacement (MR) techniques. A model containing a total of 524 polyalanine residues derived from the crystal structure of farnesyltransferase [12] was used as a search model. A molecular replacement solution was found using the program AMORE [60] of the CCP4 package [61]. The following four heavy-atom derivatives were used in MIR phasing (Table 1): K_3IrCl_6, $Hg(SCH_2CH_2COONa)_2$, di-iodobis-ethylenediamine-diplatinum(II) nitrate (PIP) and xenon. The heavy-atom sites for the Ir and xenon derivatives were found in both isomorphous and anomalous difference Patterson maps, whereas the sites in the Hg and PIP derivatives were found only by difference Fourier methods. The phases from the MR solution were used to locate heavy-atom sites in the four derivatives and to bring them to the same origin, but were not combined with the resulting MIR phases. The heavy-atom parameters were refined and MIR phases were calculated using the program MLPHARE [61,62]. The final figure of merit was 0.39 for date up to 2.5 Å resolution. The phases were significantly improved by twofold molecular averaging, solvent flattening and histogram matching using the program DM [61,63].

Table 2

Refinement statistics.

Resolution range (Å)	20–2.0
Number of reflections	118,808
R_{cryst} (%)	21.8
R_{free} (%)	26.3
Protein atoms	14,185
Zinc atoms	2
Water molecules	830
Rmsd bond lengths (Å)	0.016
Rmsd bond angles (°)	1.8

Model building and refinement

The density modified MIR map was readily interpretable and an atomic model was build into the density at 2.5 Å resolution using the program O [64]. The refinement was monitored by the R_{free} [65] computed with 5% of the data randomly selected and removed from the refinement. All steps of the following refinement were done including all low-resolution data and with a bulk-solvent correction. Initially, a strong noncrystallographic symmetry (NCS) restraint was applied to the two molecules in the asymmetric unit. The initial model with an R factor of 0.47 was first refined using the program REFMAC [66] with an overall B-factor refinement using data up to 2.5 Å resolution. This led to a drop of R_{work} to 0.37 and R_{free} to 0.42. This model was then subjected to a simulated annealing procedure in CNS_0.3 [67] followed by grouped B-factor refinement and individual B-factor refinement. This led to an improvement of R_{work} to 0.30 and R_{free} to 0.37. Several rounds of manual rebuilding followed by restrained refinement in REFMAC reduced R factors to 0.27 for R_{work} and 0.31 for R_{free}. At this point all data up to 2.0 Å resolution were included in the refinement. It became clear that certain regions in the two molecules deviate from the strict NCS, and the NCS restrains were thus abandoned. Further refinement and rebuilding resulted in R_{work}/R_{free} to be 0.25/0.30, respectively. At this stage, solvent molecules were gradually included in the model using the WATERPICK routine in CNS. The final model contains the complete α subunit (residues 1–567) and 329 residues (residues 3–331) of the β subunit. Several loop regions have high B factors approaching 100 Å^2, indicating disorder. These regions include residues 8α to 25α, 192α to 199α, and 33β to 39β. Refinement statistics are summarized in Table 2.

Accession numbers

Refined atomic coordinates of RabGGT have been deposited with the Protein Data Bank under accession code 1DCE.

Supplementary material

Supplementary material including a stereoview C_α trace of RabGGT and a stereoview of the molecular surface of RabGGT is available at http://current-biology.com/supmat/supmatin.htm.

Acknowledgements

We thank Yoga Chelliah for excellent technical assistance, Nick Grishin for help with sequence alignments, data collection and stimulating discussions, Mischa Machius for critical reading of the manuscript, John Hunt, Lothar Esser, Susan Buchanan, Di Xia and Gabby Rudenko for helpful discussions, and Zbyszek Otwinowski and Andrzej Joachimiak for help with data collection and processing at the Advanced Photon Source. This work was supported by NIH grant HL20498 (MCS). MCS is a Pew Scholar in the Biomedical Sciences.

References

1. Glomset, J.A. & Farnsworth, C.C. (1994). Role of protein modification reactions in programming interactions between Ras-related GTPases and cell membranes. *Annu. Rev. Cell Biol.* **10**, 181-205.
2. Schafer, W.R. & Rine, J. (1992). Protein prenylation: genes, enzymes, targets and function. *Annu. Rev. Genet.* **26**, 209-237.
3. Marshall, C.J. (1993). Protein prenylation: a mediator of protein–protein interactions. *Science* **259**, 1865-1866.
4. Seabra, M.C. (1998). Membrane association and targeting of prenylated Ras-like GTPases. *Cell. Signal.* **10**, 167-172.
5. Zhang, F.L. & Casey, P.J. (1996). Protein prenylation: molecular mechanisms and functional consequences. *Annu. Rev. Biochem.* **65**, 241-269.
6. Casey, P.J. & Seabra, M.C. (1996). Protein prenyltransferase. *J. Biol. Chem.* **271**, 5289-5292.
7. Omer, C.A. & Gibbs, J.B. (1994). Protein prenylation in eukaryotic microorganisms: genetics, biology and biochemistry. *Mol. Microbiol.* **11**, 219-225.
8. Seabra, M.C., Reiss, Y., Casey, P.J., Brown, M.S. & Goldstein, J.L. (1991). Protein farnesyltransferase and geranylgeranyltransferase share a common α subunit. *Cell* **65**, 429-434.
9. Brown, M.S., Goldstein, J.L., Paris, K.J., Burnier, J.P. & Marsters, J.C., Jr. (1992). Tetrapeptide inhibitors of protein farnesyltransferase: amino-terminal substitution in phenylalanine-containing tetrapeptides restores farnesylation. *Proc. Natl Acad. Sci. USA* **89**, 8313-8316.
10. Goldstein, J.L., Brown, M.S., Stradley, S.J., Reiss, Y. & Gierasch, L.M. (1991). Nonfarnesylated tetrapeptide inhibitors of protein farnesyltransferase. *J. Biol. Chem.* **266**, 15575-15578.
11. Reiss, Y., Goldstein, J.L., Seabra, M.C., Casey, P.J. & Brown, M.S. (1990). Inhibition of purified p21ras farnesyl:protein transferase by Cys–AAX tetrapeptides. *Cell* **62**, 81-88.
12. Park, H.W., Boduluri, S.R., Moomaw, J.F., Casey, P.J. & Beese, L.S. (1997). Crystal structure of protein farnesyltransferase at 2.25 angstrom resolution. *Science* **275**, 1800-1804.
13. Dunten, P., Kammlott, U., Crowther, R., Weber, D., Palermo, R. & Birktoft, J. (1998). Protein farnesyltransferase: structure and implication for substrate binding. *Biochemistry* **37**, 7907-7912.
14. Long, S.B., Casey, P.J. & Beese, L.S. (1998). Cocrystal structure of protein farnesyltransferase complexed with a farnesyl diphosphate substrate. *Biochemistry* **37**, 9612-9618.
15. Strickland, C.L., *et al*., & Weber, P.C. (1998). Crystal structure of farnesyl protein transferase complexed with a CaaX peptide and farnesyl diphosphate analogue. *Biochemistry* **37**, 16601-16611.
16. Brown, M.S. & Goldstein, J.L. (1993). Protein prenylation. Mad bet for Rab. *Nature* **366**, 14-15.
17. Pfeffer, S.R. (1994). Rab GTPases: master regulators of membrane trafficking. *Curr. Opin. Cell Biol.* **6**, 522-526.
18. Novick, P. & Zerial, M. (1997). The diversity of Rab proteins in vesicle transport. *Curr. Opin. Cell Biol.* **9**, 496-504.
19. Farnsworth, C.C., Seabra, M.C., Ericsson, L.H., Gelb, M.H. & Glomset, J.A. (1994). Rab geranylgeranyl transferase catalyzes the geranylgeranylation of adjacent cysteines in the small GTPases Rab1A, Rab3A, and Rab5A. *Proc. Natl Acad. Sci. USA* **91**, 11963-11967.
20. Anant, J.S., *et al*., & Seabra, M.C. (1998). Mechanism of Rab geranylgeranylation: formation of the catalytic ternary complex. *Biochemistry* **37**, 12559-12568.
21. Seabra, M.C., Goldstein, J.L., Südhof, T.C. & Brown, M.S. (1992). Rab geranylgeranyl transferase. A multisubunit enzyme that prenylates GTP-binding proteins terminating in Cys–*X*–Cys or Cys–Cys. *J. Biol. Chem.* **267**, 14497-14503.
22. Seabra, M.C., Brown, M.S., Slaughter, C.A., Südhof, T.C. & Goldstein, J.L. (1992). Purification of component A of Rab geranylgeranyl transferase: possible identity with the choroideremia gene product. *Cell* **70**, 1049-1057.
23. Alexandrov, K., Horiuchi, H., Steele-Mortimer, O., Seabra, M.C. & Zerial, M. (1994). Rab escort protein-1 is a multifunctional protein that accompanies newly prenylated rab proteins to their target membranes. *EMBO J.* **13**, 5262-5273.
24. Wilson, A.L., Erdman, R.A. & Maltese, W.A. (1996). Association of Rab1B with GDP-dissociation inhibitor (GDI) is required for recycling but not initial membrane targeting of the Rab protein. *J. Biol. Chem.* **271**, 10932-10940.
25. Anderson, T.A., Levitt, D.G. & Banaszak, L.J. (1998). The structural basis of lipid interaction in lipovitellin, a soluble lipoprotein. *Structure* **6**, 895-909.
26. Raag, R., Appelt, K., Xuong, N.H. & Banaszak, L. (1988). Structure of the lamprey yolk lipid–protein complex lipovitellin-phosvitin at 2.8 Å resolution. *J. Mol. Biol.* **200**, 553-569.
27. Thunnissen, A.-M.W.H., *et al*., & Dijkstra, B.W. (1994). Doughnut-shaped structure of a bacterial muramidase revealed by X-ray crystallography. *Nature* **367**, 750-753.
28. Das, A.K., Cohen, P.W. & Barford, D. (1998). The structure of the tetratricopeptide repeats of protein phosphatase 5: implications for TPR-mediated protein–protein interactions. *EMBO J.* **17**, 1192-1199.
29. Zhang, H. & Grishin, N.V. (1999). The α-subunit of protein prenyltransferases is a member of the tetratricopeptide family. *Protein Sci.* **8**, 1658-1667.
30. Holm, L. & Sander, C. (1993). Protein structure comparison by alignment of distance matrices. *J. Mol. Biol.* **233**, 123-138.
31. Jacobson, R.H., Zhang, X.-J., DuBose, R.F. & Matthews, B.W. (1994). Three-dimensional structure of β-galactosidase from *E. coli*. *Nature* **369**, 761-766.
32. Deisenhofer, J. (1981). Crystallographic refinement and atomic models of a human Fc fragment and its complex with fragment B of protein A from *Staphylococcus aureus* at 2.9 and 2.8 Å resolution. *Biochemistry* **20**, 2361-2370.
33. Sutton, R.B., Davletov, B.A., Berghuis, A.M., Südhof, T.C. & Sprang, S.R. (1995). Structure of the first C_2 domain of synaptotagmin I: a novel Ca^{2+}/phospholipid-binding fold. *Cell* **80**, 929-938.
34. Bork, P., Holm, L. & Sander, C. (1994). The immunoglobulin fold: structural classification, sequence patterns and common core. *J. Mol. Biol.* **242**, 309-320.
35. Kobe, B. & Deisenhofer, J. (1993). Crystal structure of porcine ribonuclease inhibitor, a protein with leucine-rich repeats. *Nature* **366**, 751-756.
36. Kajava, A.V. (1998). Structural diversity of leucine-rich repeat proteins. *J. Mol. Biol.* **277**, 519-527.
37. Kajava, A.V., Vassart, G. & Wodak, S.J. (1995). Modeling of the three-dimensional structure of proteins with the typical leucine-rich repeats. *Structure* **3**, 867-877.
38. Price, S.R., Evans, P.R. & Nagai, K. (1998). Crystal structure of the spliceosomal U2B′′–U2A′ protein complex bound to a fragment of U2 small nuclear RNA. *Nature* **394**, 645-650.
39. Wendt, K.U., Poralla, K. & Schulz, G.E. (1997). Structure and function of a squalene cyclase. *Science* **277**, 1811-1815.
40. Nagar, B., Jones, R.G., Diefenbach, R.J., Isenman, D.E. & Rini, J.M. (1998). X-ray crystal structure of C3d: a C3 fragment and ligand for complement receptor 2. *Science* **280**, 1277-1281.
41. Alzari, P.M., Souchon, H. & Dominguez, R. (1996). The crystal structure of endoglucanase CelA, a family 8 glycosylhydrolase from *Clostridium thermocellum*. *Structure* **4**, 265-275.
42. Pompliano, D.L., Rands, E., Schaber, M.D., Mosser, S.D., Anthony, N.J. & Gibbs, J.B. (1992). Steady-state kinetic mechanism of Ras farnesyl–protein transferase. *Biochemistry* **31**, 3800-3807.
43. Pompliano, D.L., Schaber, M.D., Mosser, S.D., Omer, C.A., Shafer, J.A. & Gibbs, J.B. (1993). Isoprenoid diphosphate utilization by recombinant human farnesyl–protein transferase: interactive binding between substrates and a preferred kinetic pathway. *Biochemistry* **32**, 8341-8347.
44. Furfine, E.S., Leban, J.J., Landavazo, A., Moomaw, J.F. & Casey, P.J. (1995). Protein farnesyltransferase: kinetics of farnesyl pyrophosphate binding and product release. *Biochemistry* **34**, 6857-6862.
45. Huang, C.C., Casey, P.J. & Fierke, C.A. (1997). Evidence for a catalytic role of zinc in protein farnesyltransferase. Spectroscopy of Co^{2+}-farnesyltransferase indicates metal coordination of the substrate thiolate. *J. Biol. Chem.* **272**, 20-23.

46. Tschantz, W.R., Furfine, E.S. & Casey, P.J. (1997). Substrate binding is required for release of product from mammalian protein farnesyltransferase. *J. Biol. Chem.* **272**, 9989-9993.
47. Desnoyers, L. & Seabra, M.C. (1998). Single prenyl-binding site on protein prenyl transferases. *Proc. Natl Acad. Sci. USA* **95,** 12266-12270.
48. Andres, D.A., Goldstein, J.L., Ho, Y.K. & Brown, M.S. (1993). Mutational analysis of alpha-subunit of protein farnesyltransferase. Evidence for a catalytic role. *J. Biol. Chem.* **268**, 1383-1390.
49. Dolence, J.M., Rozema, D.B. & Poulter, C.D. (1997). Yeast protein farnesyltransferase. Site-directed mutagenesis of conserved residues in the beta-subunit. *Biochemistry* **36**, 9246-9252.
50. Kobe, B. & Deisenhofer, J. (1994). The leucine-rich repeat: a versatile binding motif. *Trends Biochem. Sci.* **19**, 415-421.
51. Schalk, I., *et al*., & Balch, W.E. (1996). Structure and mutational analysis of Rab GDP-dissociation inhibitor. *Nature* **381**, 42-48.
52. Fujimura, K., Tanaka, K., Nakano, A. & Toh-e, A. (1994). The *Saccharomyces cerevisiae MSI4* gene encodes the yeast counterpart of component A of Rab geranylgeranyltransferase. *J. Biol. Chem.* **269**, 9205-9212.
53. Seabra, M.C., Brown, M.S. & Goldstein, J.L. (1993). Retinal degeneration in choroideremia: deficiency of rab geranylgeranyl transferase. *Science* **259**, 377-381.
54. Cremers, F.P.M., Armstrong, S.A., Seabra, M.C., Brown, M.S. & Goldstein, J.L. (1994). REP-2, a Rab escort protein encoded by the choroideremia-like gene. *J. Biol. Chem.* **269**, 2111-2117.
55. Seabra, M.C. (1996). New insights into the pathogenesis of choroideremia: a tale of two REPs. *Ophthalmic Genet.* **17,** 43-46.
56. Seabra, M.C., Ho, Y.K. & Anant, J.S. (1995). Deficient geranylgeranylation of Ram/Rab27 in choroideremia. *J. Biol. Chem.* **270**, 24420-24427.
57. Armstrong, S.A., Brown, M.S., Goldstein, J.L. & Seabra, M.C. (1995). Preparation of recombinant Rab geranylgeranyltransferase and Rab escort proteins. *Methods Enzymol.* **257**, 30-41.
58. Otwinowski, Z. & Minor, W. (1997). Processing of X-ray diffraction data collected in oscillation mode. *Methods Enzymol.* **276**, 307-326.
59. Soltis, S.M., Stowell, M.H.B., Wiener, M.C., Phillips, G.N., Jr. & Rees, D.C. (1997). Successful flash-cooling of xenon-derivatized myoglobin crystals. *J. Appl. Crystallogr.* **30**, 190-194.
60. Navaza, J. (1994). AMoRe: an automated package for molecular replacement. *Acta Crystallogr. A* **50**, 157-163.
61. Collaborative Computational Project Number 4 (1994). The CCP4 suite: programs for protein crystallography. *Acta Crystallogr. D* **50**, 760-763.
62. Otwinowski, Z. (1991). Maximum-likelihood refinement of heavy atom parameters. In *Isomorphous Replacement and Anomalous Scattering.* In *Proceedings of the CCP4 study weekend 25-26 January 1991.* (Wolf, W., Evans, P.R. & Leslie, A.G.W. eds), pp. 80-86, SERC Daresbury Laboratory, Warrington, UK.
63. Cowtan, K.D. & Main, P. (1996). Phase combination and cross validation in iterated density-modification calculations. *Acta Crystallogr. D* **52**, 43-48.
64. Jones, T.A., Zou, J.-Y., Cowan, S.W. & Kjeldgaard, M. (1991). Improved methods for building protein models in electron density maps and the location of errors in these models. *Acta Crystallogr. A* **47**, 110-119.
65. Brünger, A.T. (1992). Free R value: a novel statistical quantity for assessing the accuracy of crystal structures. *Nature* **355**, 472-475.
66. Murshudov, G.N., Vagin, A.A. & Dodson, E.J. (1997). Refinement of macromolecular structures by the maximum-likelyhood method. *Acta Crystallogr. D* **53**, 240-255.
67. Brünger, A.T., *et al*., & Warren, G.L. (1998). Crystallography and NMR system: a new software suite for macromolecular structure determination. *Acta Crystallogr. D* **54**, 905-921.

Because *Structure with Folding & Design* operates a 'Continuous Publication System' for Research Papers, this paper has been published on the internet before being printed (accessed from http://biomednet.com/cbiology/str). For further information, see the explanation on the contents page.